Article

Characterization of Anion Exchange Membrane Containing Epoxy Ring and C–Cl Bond Quaternized by Various Amine Groups for Application in Fuel Cells

Sung Kuk Jeong, Ju Sung Lee, Sahng Hyuck Woo, Jin Ah Seo and Byoung Ryul Min *

Department of Chemical and Biomolecular Engineering, Yonsei University, 50 Yonsei-ro, Seodaemun-gu, Seoul 120-749, Korea; E-Mails: lynx0419@yonsei.ac.kr (S.K.J.); smilelee2@naver.com (J.S.L.); korwsh@yonsei.ac.kr (S.H.W.); doublej201@yonsei.ac.kr (J.A.S.)

* Author to whom correspondence should be addressed; E-Mail: minbr345@yonsei.ac.kr; Tel.: +82-2-2123-2757; Fax: +82-2-312-6401.

Abstract: Anion exchange membranes were synthesized from different compositions of glycidyl methacrylate (GMA) and vinylbenzyl chloride (VBC), with constant content of divinyl benzene (DVB) by radical polymerization using benzoyl peroxide (BPO) on non-woven polyethylene terephthalate (PET) substrate. Polymerized membranes were then quaternized by soaking in trimethylamine (TMA), triethylamine (TEA), tripropylamine (TPA), and 1,4-diazabicyclo [2.2.2] octane (DABCO). Characteristics of membranes were confirmed by Fourier transform infrared spectroscopy, water uptake, ion exchange capacity, ion conductivity, thermal, and alkaline stability. The results revealed that membranes quaternized by TPA and DABCO showed high affinity when GMA content was 15 wt% and 75 wt%, respectively. IEC and ion conductivity of membranes quaternized by TPA were 1.34 meq·g^{-1} and 0.022 S·cm^{-1} (at 60 °C), respectively. IEC and ion conductivity of membranes were quaternized by DABCO were 1.34 meq·g^{-1} and 0.021 S·cm^{-1} (at 60 °C), respectively. The results indicate that the membrane containing GMA 15 wt% quaternized by TPA showed the highest thermal stability among membranes and exhibited high ion conductivity compared to existing researches using GMA, VBC, and DVB monomers.

Keywords: fuel cell; glycidyl methacrylate; divinyl benzene; vinyl benzyl chloride; anion exchange membrane

1. Introduction

Membrane technology has been actively developed and used in a wide range of applications in fuel cells, water treatment, and biotechnology [1–3]. The fuel cells are the most important among those applications because they are effective devices for alleviating carbon dioxide emission from combustion such as cars and power plants. The energy sources of fuel cells are hydrogen and methanol, which do not originated from fossil fuel, making fuel cells environmentally friendly [4,5]. Moreover, energy efficiency of fuel cells is higher than conventional energy devices such as diesel and gasoline engines operating on fossil fuel. Emergence of fuel cells has been led by discovery of new materials and new technologies. There are several types of fuel cells, but anion exchange membrane fuel cells (AEMFCs) provide advantages compared to other fuel cells. Basically, AEMFCs use anion exchange membranes as separator, which transport hydroxide from cathode side to anode side, provide potassium hydroxide as electrolyte, and convert hydrogen directly to electrical current. Their advantages include the following: (1) oxygen reduction kinetics happen more readily in alkaline conditions than in acidic conditions, and thus the amount of highly expensive catalysts used such as platinum can be decreased; (2) their operating temperature is relatively low, in the 60 to 90 °C range; (3) corrosion problems are alleviated under alkaline conditions; and (4) hydrogen, the fuel for AEMFCs, can be replaced by liquid fuels such as methanol, ethanol, and propanol due to high anode potential to oxidize C-C bonds in alcohol [6]. However, the anion exchange membranes (AEM) in AEMFCs have poor chemical stability in high pH environments, so their performance can be limited. To be more specific, cation sites, which are generated from quaternized ammonium groups on the membrane, can be decomposed as the hydroxides move through the membrane. Hoffman degradation (E2 elimination), E1 elimination, and nucleophilic substitution (S_N2) can occur to break up quaternized amines when ammonium groups are exposed in hydroxide solutions [7–9]. Therefore, ion conductivity and alkaline stability gradually decline in alkaline environment. Glycidyl methacrylate monomer, vinylbenzyl chloride monomer, and divinyl benzene monomer have been studied as alternatives to improve chemical stability for anion exchange membrane [10,11]. Glycidyl methacrylate (GMA) monomer contains acrylic and epoxy, and provides good flexibility in polymer structure. The epoxy groups in this monomer can react with other functional groups such as carboxyl, hydroxyl, and amine groups. GMA monomer has been known to lead a significant increase in polymerization rate and improve the wet-strength of the resulting polymer [12,13]. Vinylbenzyl chloride (VBC) is also used as a polymer reactant and polymeric support. VBC is a dual functional monomer with C=C and C–Cl structures, which means that VBC may be polymerized by itself and also react with amine groups. As for divinyl benzene (DVB), there is a need for its polymer structure to be held because the solubility of polymer prevents its application in AEMFCs. It was reported that the components of DVB, acting as cross-linker among monomers, affects ion conductivity, thermal stability, and chemical stability [14]. All monomers (GMA, DVB, and VBC) are oil-phase, meaning that these monomers can be mixed. Non-woven PET was introduced to anion exchange membranes due to its chemically inert property and high tensile strength. In addition, non-woven PET has good permeability due to high porosity. Benzoyl peroxide (BPO) can initiate radical polymerization among GMA, DVB, and VBC due to the C=C structure. There has been much research on polymerization of GMA-DVB, VBC-DVB, and GMA-VBC, respectively [15,16]. The conductivity of copolymer of poly (methyl methacrylate-co-butyl acrylate-co-vinylbenzyl chloride) reached 8.2×10^{-3} S·cm^{-1} at

80 °C [17]. Organic-inorganic hybrid membranes applying VBC showed 8.2 × 10^{-3} S·cm^{-1} and thermally endured 150 °C without decomposition of amine [18]. Poly(GMA-DVB) and poly(VBC-DVB) exhibited membrane resistance 1.5 and 1.2 Ω·cm^2 respectively [11]. However, ion conductivity and thermal stability such studies were not efficient during fuel cell tests. If these two factors are improved, performance of AEMFCs will be improved. Although these experiments have been conducted, apparently none has been conducted on poly (GMA-DVB-VBC). In addition, this study attempts to fill monomers in non-woven PET, which is also unprecedented.

The purpose of this study is to fabricate anion exchange membranes with different compositions of monomers (GMA and VBC) at constant DVB content level on non-woven PET substrate, and by quaternizing anion exchange membranes with various amine functional groups such as TMA, TEA, TPA, and DABCO. It was expected that membranes containing both epoxy ring and C–Cl, which react when nucleophilic amine groups are introduced, would present high ion conductivity and chemical stability. It was also anticipated that each monomer would display advantages at certain compositions. To begin with, polymerization of membranes was measured FTIR. The water uptake, IEC, ion conductivity, activation energy of quaternized membrane, Thermo gravimetric analysis (TGA), and alkaline stability were measured for membrane performance.

2. Experimental Section

2.1. Materials

Glycidyl methacrylate (GMA, Fluka, Japan), 4-vinylbenzyl chloride (VBC, Aldrich, St. Louis, MO, USA) were used as monomers. Divinyl benzene (DVB, Fluka, Tokyo, Japan) was used as cross-linker. Benzoyl peroxide (BPO, Fluka, Japan) was used as an initiator. Trimethylamine (TMA, Sigma Aldrich, St. Louis, MO, USA), trimethylamine (TEA, Sigma Aldrich), tripropylamine (TPA, Sigma Aldrich), and 1, 4-diazabicyclo [2.2.2] octane (DABCO, Sigma Aldrich) were used for the amination process. Potassium hydroxide (KOH, SK chemical, Seoul, Korea) was used. The non-woven poly ethylene terephthalate (PET) with a thickness of 0.1 mm was used as a support structure for monomer reaction and was purchased from Philos (Kunposi, Korea).

2.2. Membrane Preparation

DVB, GMA, and VBC were set under the compositions listed in Table 1 for the preparation of base membranes. BPO was applied at 2 wt% with respect to the total amount of monomers used. Monomer solutions with BPO were mixed in a glass bottle and stirred under the nitrogen gas at 25 °C for 30 min to eliminate remnant oxygen in solution. Round-shaped PETs were soaked in solution for 30 min. Well-soaked non-woven PET was interlayered between two flat glasses. Thermal polymerization was performed in oven at 80 °C for 9 h. After thermal radical polymerization, base membranes (GMA + DVB + BPO + PET) were taken out from oven and dried in a petri dish at 25 °C for 6 h to remove unreacted monomers. Epoxy of GMA and C–Cl of VBC on base membranes were quaternized by soaking in TMA, TEA, TPA, and DABCO solutions, under quaternization conditions shown in Table 2. Chemical structures of GDV45 membranes based on different functional groups are presented in Figure 1. The quaternized membranes were kept in 1 M KOH solution for 24 h and washed thoroughly with

deionized water. Membranes were stored in a glass bottle filled with nitrogen gas and deionized water because hydroxide anions can transform into carbonate and bicarbonate species when they come into contact with carbon dioxide in the atmosphere [19].

Table 1. Composition of monomer solutions.

Membranes	GMA (wt%)	VBC (wt%)	DVB (wt%)
GVD75	75	15	10
GVD45	45	45	10
GVD15	15	75	10

Table 2. Recipes for quaternization of each functional group on the base membrane.

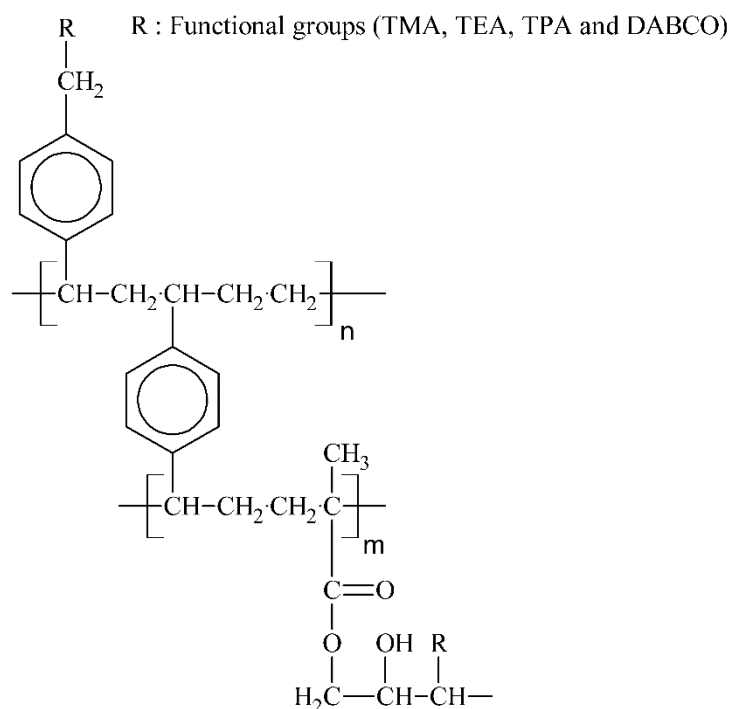| Reagent	Concentration (M)	Reaction Temperature (°C)	Reaction Time (h)
TMA	1	30	12
TEA	1	50	12
TPA	1	50	12
DABCO	1	60	12

Figure 1. Chemical structure of GDV45 membranes based on different functional groups.

2.3. Membrane Measurements

2.3.1. Morphological Evaluation

The morphology of the membrane surfaces and cross sections were analyzed at an accelerating voltage of 5 kV using a field emission scanning electron microscopy (FE-SEM, JEOL-6701F, JEOL, Tokyo, Japan). The membranes were coated with platinum (Pt) for 150 s before the SEM observation.

2.3.2. Fourier Transform Infrared Spectroscopy (FT-IR)

The chemical structure and functional group of samples were identified using FT-IR (PerkinElmer, Spectrum 100, Waltham, MA, USA). All spectra were recorded in the 4000–600 cm^{-1} range.

2.3.3. Thermal Analysis

Thermo gravimetric analysis (TGA) curves were carried out with simultaneous thermal analyzer (PerkinElmer, STA8000, Shelton, CT, USA) at the rate of 5 °C per minute under N_2 gas. This method indicates thermal property and stability of the membranes at varying temperatures.

2.3.4. Water Uptake

The weight of wet membrane (W_w) was determined after equilibrating a sample of membrane in deionized water at room temperature. The weight of dried membrane (W_d) was determined by removing surface water from the membrane by wiping and drying it over 12 h at 80 °C until weight remained unchanged. The water uptake (W_u) was then calculated based on the following Equation (1):

$$W_u = \frac{W_w - W_d}{W_d} \times 100\%$$
(1)

2.3.5. Ionic Conductivity

The design of the conductivity measurement cell is depicted in Figure 1. The conductivity of the membrane was measured by supplying alternating current (AC) with a frequency of 2 KHz through a pair of platinum electrodes. 0.1 mol·L^{-1} KOH aqueous solution was used as electrolyte in the cell. Conductivity was measured at varying temperatures. KOH aqueous solution was heated in a thermostat at certain temperatures from 20 °C to 60 °C, and poured in the cell. A low-concentration KOH was used since high-concentration KOH influences ionic conductivity at high temperatures [20,21]. The ion conductivity of the membrane (σ) was calculated by Equation (2):

$$\sigma(\text{S} \cdot \text{cm}^{-1}) = \frac{l}{R_M \times S}$$
(2)

where, l is the thickness of membrane (cm), R_M is the difference in resistance between attaching membrane and detaching membrane in the cell, and S is the membrane surface (cm^2) for hydroxide transportation. The conductivity measurement cell was depicted in Figure 2 [22].
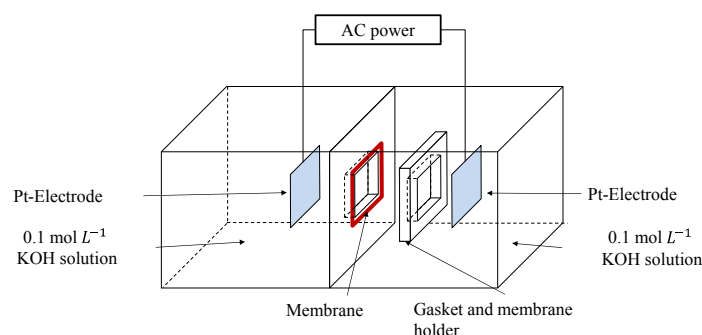

Figure 2. Scheme of the conductivity measurement cell. The effective area of the cell is 4 cm^2.

2.3.6. Ion Exchange Capacity (IEC)

Mohr method was used to measure ion exchange capacity (IEC). Fabricated membranes were dried to constant weight and then soaked in 1 mol·L^{-1} NaCl solution for 1 day to fully attach chloride ions to positive charge area of membrane. Remnant NaCl was removed by deionized water. The sample was immersed in 0.5 mol·L^{-1} NaNO$_3$ for reaching equilibrium and then took out the sample. This solution was titrated against with 0.1 mol·L^{-1} AgNO$_3$ solution using K$_2$CrO$_4$ as an indicator (1 mL). Titration was repeated three times to get an average ion exchange capacity value. Ion-exchange capacity was calculated as follows Equation (3):

$$IEC = \frac{volume\ of\ AgNO3(\text{mL}) \times concentration\ of\ AgNO3\ (\frac{\text{mmol}}{\text{mL}})}{g(weight\ of\ dry\ membrane)} \tag{3}$$

2.3.7. Membrane Stability in Alkaline Solution

IEC and conductivity of membrane were measured before and after treatment with KOH solution. Membranes were immersed in 1.0 mol·L^{-1} KOH at 60 °C for 144 h and comparative changes in IEC and conductivity were recorded after washing completely with deionized water. Conductivity was measured using the conductivity cell depicted in Figure 1.

3. Results and Discussion

3.1. SEM

Surface morphologies of the non-woven PET, GDV45 base membrane, and GDV45-TMA membrane by TMA are presented in Figure 3. Figure 3a,b is the original PET substrate and polymerized film respectively. PET substrate in Figure 3a shows many pores, but polymerized film in Figure 3b thoroughly covered pores after thermal polymerization. The bumpy polymerized film surface (Figure 3c) was flattened out by introducing amine groups (Figure 3d). Figure 3e shows the cross section image of quaternized GDV45 membrane. Middle area of Figure 3e was non-woven PET and the edge of the areas presented in Figure 3e showed polymerized film area. Several circles in middle area were not pores but traces of non-woven PET. Therefore, it was discovered that monomers (GMA, DVB, and VBC) were successfully synthesized and amine functional groups were well quaternized on the non-woven PET substrate.

3.2. FT-IR

The FTIR spectra of non-woven PET and poly (GMA-DVB-VBC) with different compositions are shown in Figure 4. The bands at 2923 and 2852 cm^{-1} are assigned to the stretching vibration of –CH$_2$ and –CH groups. The C=O (–COO– in carboxyl group) is the band at 1719 cm^{-1} and epoxy (–COC–) stretching vibration the band at 907 cm^{-1} [23,24]. The intensity of C=O and epoxy vibration bands increases as composition of GMA is increased from 15 wt% to 75 wt%. Bands at 1510 and 1608 correspond to C=C stretching vibration in aromatic ring [25]. GDV15 and GDV45 base membranes containing aromatic rings from VBC and DVB show more intensive bands compared to those of GDV75 base membrane. C–Cl stretching from VBC corresponds with the band at 1265 cm^{-1} and its intensity

increases as the composition of VBC is increased from 15 wt% to 75 wt%. [26] These results indicate that monomers (GMA, DVB, and VBC) were successfully polymerized and combined with non-woven PET.
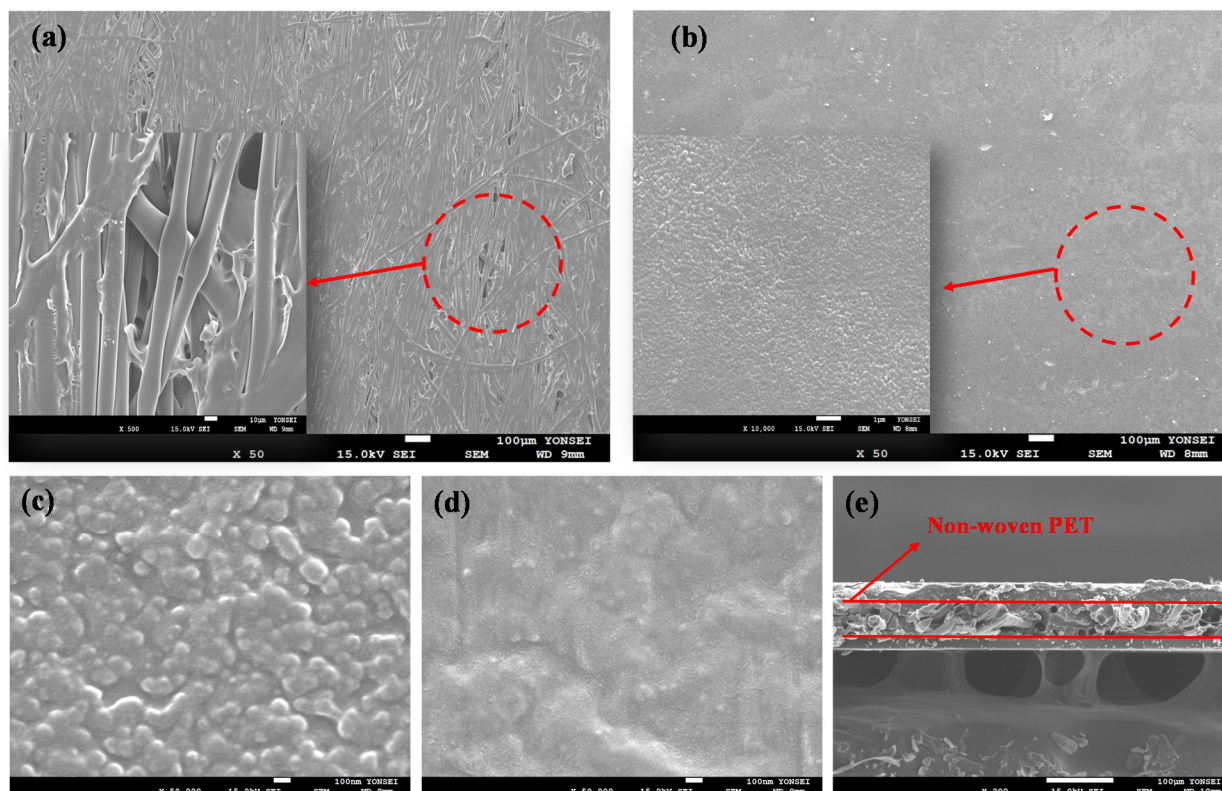

Figure 3. SEM surface images of: (**a**) non-woven PET; (**b**) GDV45 base membrane; (**c**) enlarged surface of GDV45 base membrane; and (**d**) GDV45-TMA membrane; and SEM cross section image of: (**e**) GDV45-TMA.
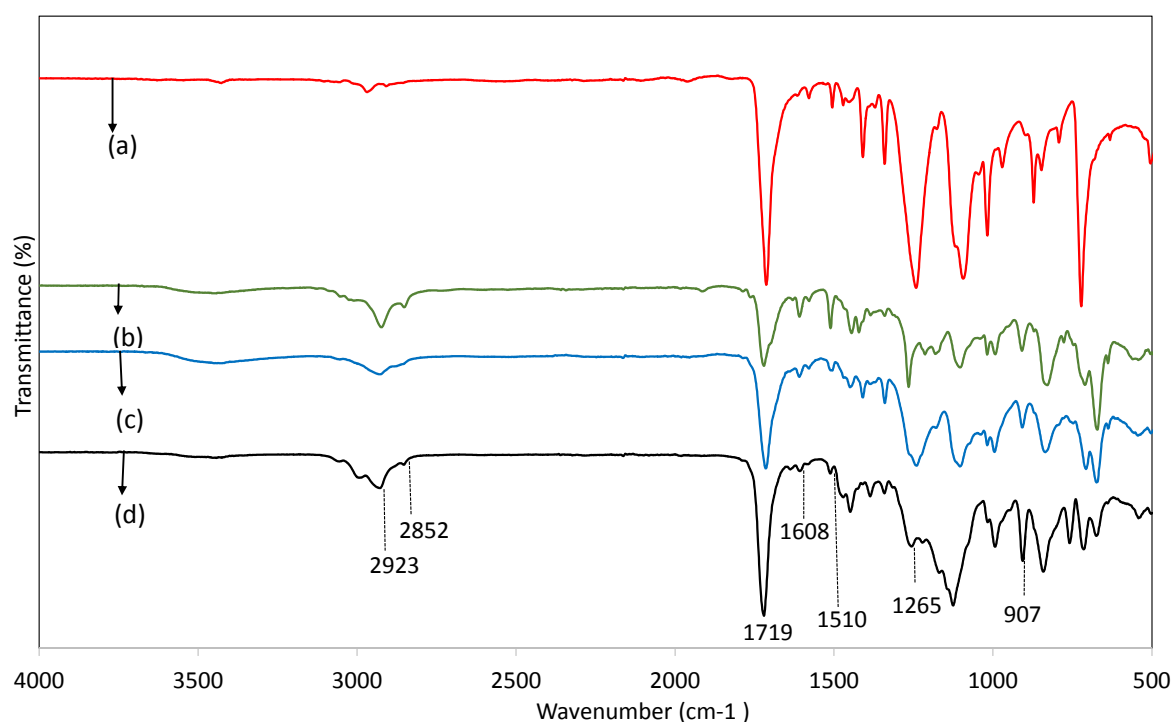

Figure 4. FT-IR spectra of (**a**) non-woven PET; (**b**) GDV75; (**c**) GDV45; and (**d**) GDV15.

Among GDV membranes with varying compositions, GDV45 base membrane and membranes combined with different functional groups (TMA, TEA, TPA, and DABCO) were analyzed by FT-IR to confirm the quaternization of membranes listed in Figure 5. GDV45 base membrane was selected to confirm quaternization because this membrane has identical weight percent ratio between GMA and VBC (Table 1). Figure 5b–e each exhibit a broad band at 3400 cm^{-1}, which are ascribed to stretching vibration of –OH groups from epoxy ring opening reaction. The C–N vibration of function groups (TMA, TEA, and TPA) show new peaks at 1170 cm^{-1}. GDV45-DABCO presents C–N vibrations near 1614 cm^{-1} and 1463 cm^{-1} [27]. The bands at 1260 cm^{-1} and 907 cm^{-1} do not disappear although amine groups are introduced to the base membrane, the reason for which will be discussed in the IEC section. The results from Figure 4 show that functional groups (TMA, TEA, TPA, and DABCO) successfully developed chemical bonding between the epoxy ring from GMA and C–Cl from VBC on base membranes.
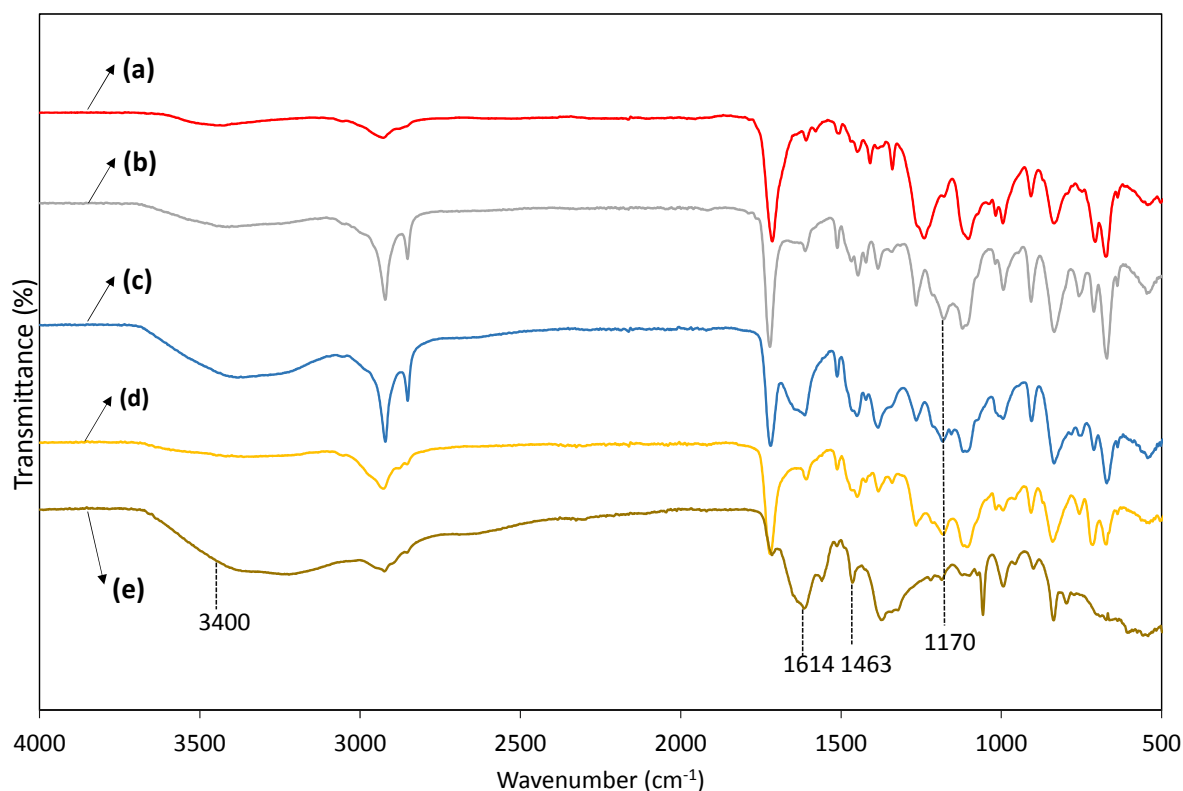

Figure 5. FT-IR spectra of (**a**) GDV45; (**b**) GDV45-TMA; (**c**) GDV45-TEA; (**d**) GDV45-TPA; and (**e**) GDV45-DABCO.

3.3. Water Uptake, Ion Exchange Capacity, and Conductivity

Water uptake, ion exchange capacity (IEC), membrane thickness, and hydroxide conductivity of each membrane are listed in Table 3. These factors are crucial parameters in judging membrane performance.

Water uptake, IEC, and ion conductivity were in the decreasing order of TPA > TMA > DABCO > TEA when the composition of GMA was 15% by weight. VBC predominates in the GDV15 base membrane because C–Cl bonds from VBC outnumber the epoxy rings from GMA. The GDV15-TPA had higher IEC (1.34 meq/g) than GDV15-DABCO (0.72 meq/g), which corresponded to change in water uptake from 38% to 21%. With abundant VBC, TMA is more favorable than DABCO on the base membrane,

indicating that the TPA, which have chain structure, can favorably react with VBC rather than DABCO, which have ring structure. In addition, water uptake and conductivity also show a proportional relationship. GDV15-TPA membrane displayed higher conductivity (0.022 S/cm) and water uptake (38%) compared to GDV15-DABCO (0.009 S/cm and 21% each). GDV15-TPA structure can contain hydroxide and transport it faster. GDV15 membrane quaternized by TPA exhibited higher IEC and ion conductivity than the ones quaternized by TMA and TEA. This result implies that TEA combines less with the base membrane due to greater steric hindrance compared to TMA and TPA, even though TMA, TEA, and TPA all consist of chain structure.

Table 3. Properties of the anion exchange membranes. Ion conductivity of non-woven PET with pure water at 60 °C was 1.52×10^{-10} S/cm.

Membrane	Water Uptake (%)	IEC (meq/g)	Membrane thickness (mm)	Conductivity (S·cm^{-1}) at 60 °C
GDV15-TMA	38	1.31	0.19	0.020
GDV15-TEA	24	0.82	0.18	0.015
GDV15-TPA	38	1.34	0.19	0.022
GDV15-DABCO	21	0.72	0.21	0.009
GDV45-TMA	35	0.98	0.19	0.019
GDV45-TEA	33	0.91	0.18	0.017
GDV45-TPA	20	0.65	0.21	0.0091
GDV45-DABCO	28	0.78	0.19	0.014
GDV75-TMA	33	0.93	0.19	0.018
GDV75-TEA	22	0.68	0.19	0.011
GDV75-TPA	31	0.89	0.18	0.016
GDV75-DABCO	41	1.34	0.17	0.021

Water uptake, IEC, and ion conductivity were in the decreasing order of TMA > TEA > DABCO > TPA when the composition of GMA was 45% by weight. Performance of GDV45-TPA membrane was the lowest among GDV45 membranes. IEC and ion conductivity of membrane quatrenized by TPA showed drastic changes from GDV15-TPA (1.34 meq/g and 0.020 S/cm) to GDV45-TPA (0.65 meq/g and 0.0091 S/cm). Therefore, the GDV45 membrane is not favorable for quaternization using TPA. The IEC and ion conductivity of GDV45-TEA showed the second strongest performance among the functional group (TMA, TEA, TPA, and DABCO) due to the steric hindrance, and hydroxide having less chance to contact positive charges on the membrane quaternized by TEA compared to TMA. The water uptake in quaternized GDV45 membranes should be higher than those of quaternized GDV15 membranes. However, the result does not show a proportional relationship between water uptake and ion conductivity. The effectiveness of cross-linker (DVB) is intensified in GDV45 base membrane to a greater extent than in the GDV15 base membrane. To be more specific, the DVB shrinks the free volume in polymer structure and its effect is maximized in GDV45 base membrane. Epoxy ring and C–Cl vibration peaks did not completely disappear in Figure 4. This is also due to the effect of cross-linker (DVB). The DVB not only maintains polymer structure but also hinders reaction sites between base membrane and functional groups (TMA, TEA, TPA, and DABCO). Therefore, it will be necessary to find the optimum quaternization process in future studies.

Water uptake, IEC, and ion conductivity were in the decreasing order of DABCO > TMA > TPA > TEA when the composition of GMA was 75% by weight. The performance of GDV75-TEA was reduced when GMA weight concentration increased from 45% to 75%. The IEC of GDV75-TEA was low, even though GDV75 base membrane had dominant epoxy rings. In other words, TEA does not have affinity with epoxy ring. Interestingly, IEC for the membranes quaternized by DABCO were in the increasing order of G75 > G45 > G15, indicating that DABCO can form C–N bond with epoxy ring from GMA more easily compared to bonding with VBC. Understandably, certain functional groups exhibit good performance depending on composition of base membrane. TPA, TMA, and DABCO presented high IEC and conductivity when base membrane contains 15%, 45%, and 75% GMA by weight, respectively. Hydroxide conductivity must have high value (0.01–0.1 S·cm^{-1}) for potential application in AEMFCs [28]. Moreover, ion exchange capacity must be above 0.9 meq·g^{-1}. Six of the membranes with acceptable IEC and conductivity in Table 3 are selected for Table 4. It is shown in Figure 6 that the conductivity of those membranes increased when temperatures increased.

Table 4. Ion exchange capacity (IEC), conductivity and activation energy of select quaternized membranes.

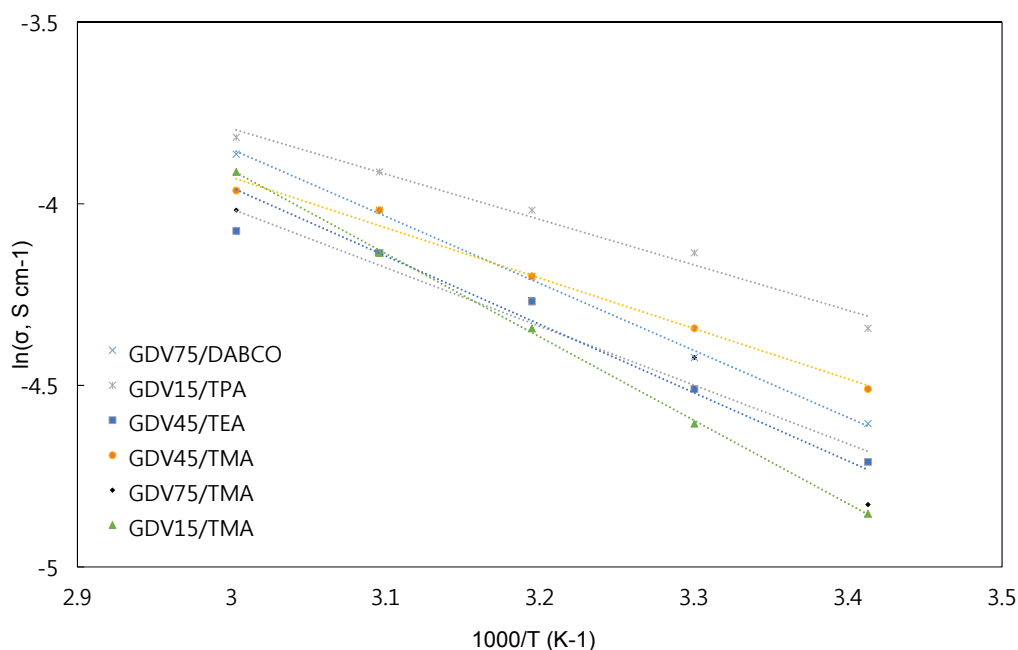| Sample	IEC (meq·g^{-1})	σ at 60°C (S·cm^{-1})	E_a (kJ·mol^{-1})
GDV15-TMA	1.31	0.020	19.10
GDV15-TPA	1.34	0.022	10.40
GDV45-TMA	0.98	0.019	11.55
GDV45-TEA	0.91	0.017	15.64
GDV75-TMA	0.93	0.018	13.44
GDV75-DABCO	1.34	0.021	15.34

Figure 6. Arrehenius plots for GDV15-TMA, GDV15-TPA, GDV45-TMA, GDV45-TEA, GDV75-TMA, and GDV75-DABCO.

Activation energy of ion transport (E_a) can be computed as $E_a = -b \times R$, where b is the slope of the linear regression (Figure 5) of lnσ *versus* 1000/T, and R is the gas constant. In other words, the Arrhenius plots of the ion conductivity of each membrane as function of temperature can be used to compute the activation energy of ion transport (E_a). Activation energy accords with energy barrier of anion migration from one point to another based on the Grotthuss mechanism [29,30]. Hydroxide transport is facilitated when the activation energy is low. The E_a of promising membranes are listed in Table 4, and varies from 10.40 to 19.10 kJ·mol^{-1}. E_a of GDV15-TPA and GDV45-TMA are smaller than other membranes listed in Table 4. In other words, membranes with high VBC composition bonding with TMA and TPA makes anion transport easier and provides more desirable cation sites than others. Therefore, GDV15-TPA and GDV45-TMA membranes are the best candidates from the perspective of water uptake, IEC, hydroxide conductivity, and activation energy.

3.4. Thermal Stability

The thermal stability of promising membranes from Table 4 was measured by thermos gravimetric analysis (TGA). Figure 7 shows TGA curves for the non-woven PET, GDV15-TMA, GDV15-TPA, GDV45-TMA, GDV45-TEA, GDV75-TMA, and GDV75-DABCO which were recorded under nitrogen gas from 30 °C to 900 °C. Weight ratio of polymer network to non-woven PET was nearly 1.3:1, although the composition of monomers was varied. Non-woven PET presented a single-step decomposition and endured up to 370 °C due to its strong chemical structure. Non-woven PET, which is coated by polymer exhibited two step decomposition. The slight mass loss below 120 °C was due to evaporation of water absorbed in the GDV15-TMA, GDV15-TPA, GDV45-TMA, GDV45-TEA, GDV75-TMA, and GDV75-DABCO membranes. The mass loss in quaternary ammonium (TMA, TEA and TPA) occurred in the 200–280 °C range. The mass loss in the 280–470 °C range was due to the degradation of polymer backbone (GDV15-TMA, GDV15-TPA, GDV45-TMA, GDV45-TEA and GDV75-TMA). Membranes which had quaternary ammonium (TMA, TEA and TPA) showed weight loss at mostly the same stage. However, mass loss in the diammonium (DABCO) was observed in the 130–250 °C range. The mass loss in the 250–450 °C range was due to the degradation of polymer backbone (GDV75-DABCO). Membranes quaternized by DABCO were relatively unstable compare to those quaternized by TMA, TEA, and TPA. All membranes listed in Table 4 showed thermal stability, with 5% mass loss in the 150–370 °C range. Ammonium functional groups (TMA, TEA, and TPA) are stable up to 200 °C, whereas diammonium functional group (DABCO) is stable up to 130 °C [31]. Therefore, these functional groups collapse when membranes are exposed at over 200 °C and at 130 °C over a long time, respectively. GDV45-TMA exhibited the highest thermal stability, but GDV15-TPA and GDV75-DABCO showed the lowest thermal stability among the membranes. Therefore, TMA functional group with low GMA content displayed the strongest thermal stability compared to other functional groups.
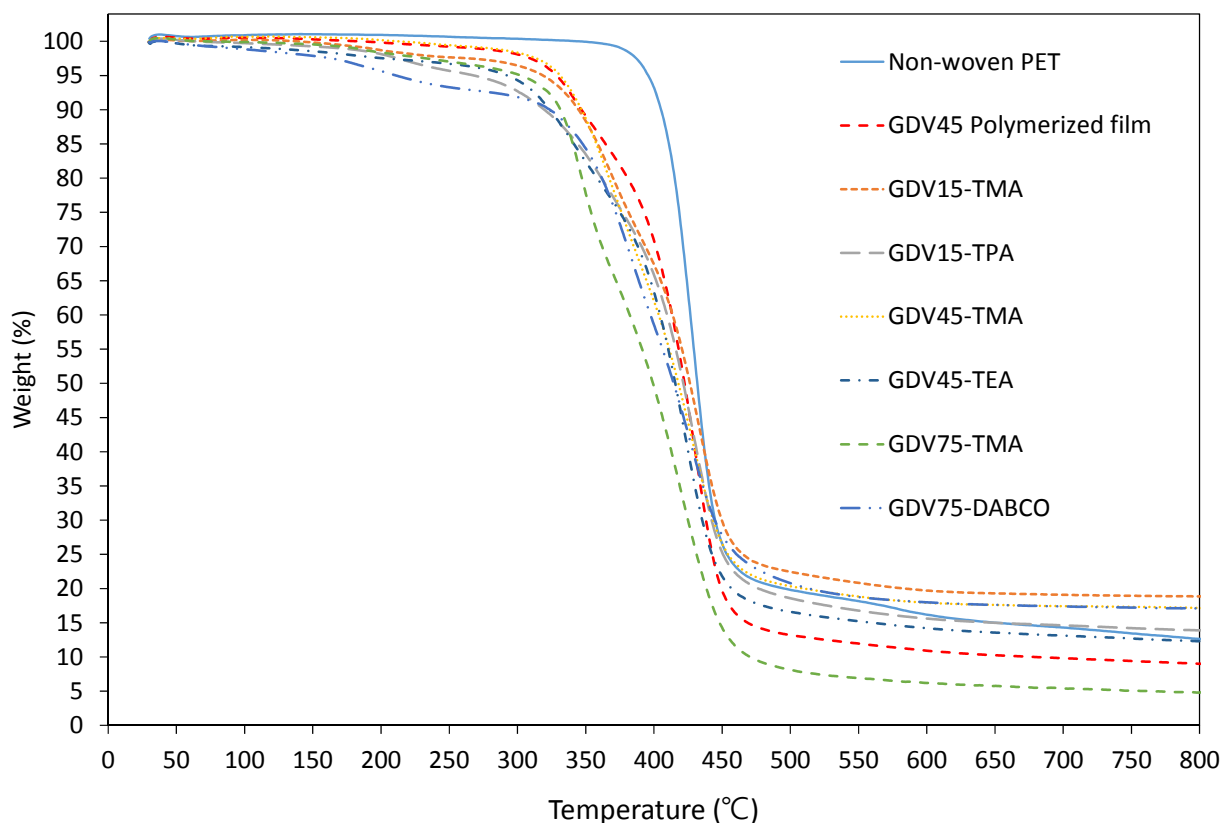
Figure 7. TGA (thermo gravimetric analysis) curves for the Non-woven PET, GDV45 base membrane, GDV15-TMA, GDV15-TPA, GDV45-TMA, GDV45-TEA, GDV75-TMA, and GDV75-DABCO.

3.5. Alkaline Stability

Anion exchange membranes are required to endure extreme alkaline conditions and temperature ranges from 60 °C from 80 °C [32]. Membranes listed in Table 4 were soaked in 1 mol/L KOH at 60 °C for 144 h and monitored for relative variation on IEC and conductivity. The results are listed in Figure 8. GDV15-TMA, GDV45-TMA, and GDV75-TMA membranes are vulnerable to nucleophilic attack by hydroxide because those membranes contain benzyltrimethylammonium, benzyltriethylammonium, and benzyltripropylammonium cations [33,34]. Therefore, IEC and conductivity decreased as time passed. IEC and conductivity of GDV75-TMA decreased slightly compared to GDV45-TMA and GDV15-TMA. TMA sustains bonding with base membrane when GMA concentration is high. In other words, nucleophilic attack by hydroxide occurs more at cation sites of VBC than cation sites of GMA. GDV15-TPA had higher IEC and conductivity than GDV15-TMA after treatment, and GDV45-TEA was more stable than GDV45-TMA due to the chain length of functional groups. Managing chain length of functional groups is one method to prevent hydroxide intrusion. Hydroxide ions cannot freely reach β-hydrogen sites on the basis of nitrogen cation when functional group is bulky. However, GDV75-TMA presented slighter changes in IEC (78%) and conductivity (64%) compared to DABCO (55% and 40% respectively) after the test. The reason that quaternized membranes based on DABCO showed weak alkaline stability is as follows. The DABCO combines epoxide rings and C–Cl bonds from the base membrane in two forms of bis-quaternized DABCO membrane and mono-quaternized DABCO membrane [35]. The DABCO can be a cross-linker when the amount of DABCO is higher than the

amount of the C–Cl bond. However, two forms of DABCO mentioned above coexist in the quaternized membrane. The bis-quaternized DABCO membrane, which serves as cross-linker was more chemically unstable than the mono-quaternized DABCO membrane [36]. Mono-quaternized DABCO are then destroyed after bis-quaternized DABCO collapse because hydroxide can approach positively charged DABCO when bis-quaternized DABCO disappears. It was known that bonding VBC with DABCO showed resistance in alkaline condition due to steric hindrance. However, bonding epoxy with DABCO easily degraded in alkali environment when epoxy of GMA was relatively high in the membrane. It indicates that combination of epoxy with DABCO is easily exposed to hydroxide ion attack compared to the combination of VBC with DABCO. In the end, IEC and conductivity decline in GDV75-DABCO membrane. Chain structure functional groups (TMA, TEA, and TPA) are more desirable than heterocyclic structure functional groups (DABCO) for long exposure in hydroxide solution. Still, further investigation of the nucleophilic attack mechanism on each of the membranes are needed. According to alkaline resistance results, GDV15-TPA and GDV75-TMA membranes have the highest tolerance to alkaline solutions among membranes. Therefore, tracking the progress of alkaline stability at high temperatures (over 60 °C) is required in further work.
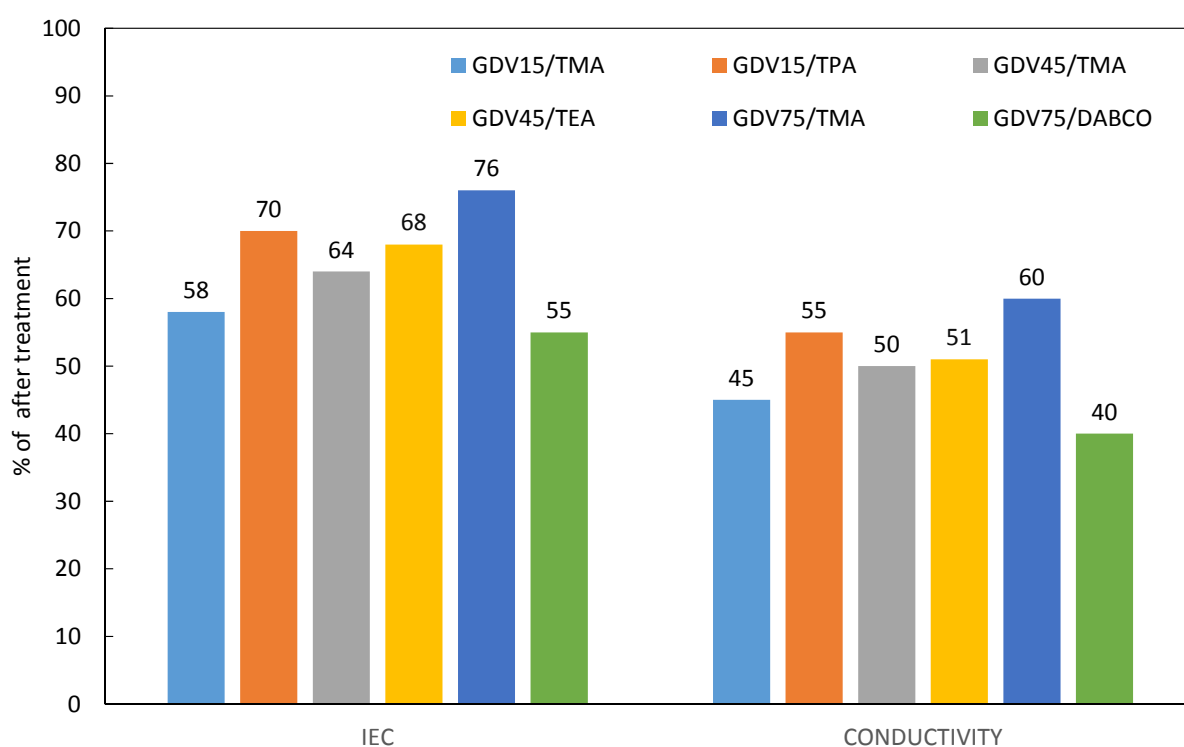

Figure 8. Changes in IEC and conductivity of the select membranes with alkaline stability test at 60 °C for 144 h.

4. Conclusions

In this study, anion exchange membranes were fabricated with different combinations of GMA, DVB, VBC, and non-woven PET, and functionalized by introducing various amine groups (TMA, TEA, TPA, and DABCO). Water uptake, IEC, ion conductivity, activation energy, thermal stability, and alkaline stability of membranes were investigated for possibility of application in AEMFCs. General relations among water uptake, IEC, and ion conductivity were verified. When VBC contents predominate in the

membrane, TPA shows high IEC and conductivity (1.34 meq·g^{-1} and 0.022 S·cm^{-1}), whereas when GMA content is high, the DABCO shows high IEC and conductivity (1.34 meq·g^{-1} and 0.021 S·cm^{-1}). Membranes quaternized by TMA and TPA with low GMA content are the best candidates considering activation energy (10.40–11.65 kJ·mol^{-1}). Chain structure ammoniums (TMA, TEA, and TPA) thermally endure up to 200 °C, while heterocyclic structure ammonium (DABCO) thermally endure up to 130 °C. In particular, TMA with low GMA content shows the highest thermal stability. The TPA reacted with membrane containing 15% GMA by weight and TMA reacted with membrane containing 75% VBC by weight present favorable alkaline stability. Based on characterizations, it is suggested that mono-ammonium groups allow membranes to improve thermal stability. When all the results are comprehensively considered, the GDV15-TPA membrane appears to have the highest applicability for AEMFCs because of having high ion conductivity and thermal resistance in comparison to existing relative researches. Further research will focus on assembling a membrane electrode assembly (MEA) and testing the power density of AEMFCs.

Acknowledgments

Author Contributions

Sung Kuk Jeong performed the experiments, synthesized membranes, and wrote first draft; Ju Sung Lee, Sahng Hyuck Woo, Jin Ah Seo analyzed the data; ByoungRyul Min revised the manuscript.

Conflicts of Interest

The authors declare no conflict of interest.

References

1. Zhang, H.; Shen, P.K. Advances in the high performance polymer electrolyte membranes for fuel cells. *Chem. Soc. Rev.* **2012**, *41*, 2382–2394.
2. Kreuer, K.D. Ion conducting membranes for fuel cells and other electrochemical devices. *Chem. Mater.* **2014**, *26*, 361–380.
3. Woo, S.H.; Park, J.; Min, B.R. Relationship between permeate flux and surface roughness of membranes with similar water contact angle values. *Sep. Purif. Technol.* **2015**, *146*, 187–191.
4. Zeng, K.; Zhang, D. Recent progress in alkaline water electrolysis for hydrogen production and applications. *Prog. Energy Combust. Sci.* **2010**, *36*, 307–326.
5. Pletcher, D.; Li, X. Prospects for alkaline zero gap water electrolysers for hydrogen production. *Int. J. Hydrogen Energy* **2011**, *36*, 15089–15104.
6. Jaeger, W.; Bohrisch, J.; Laschewsky, A. Synthetic polymers with quaternary nitrogen atoms-synthesis and structure of the most used type of cationic polyelectrolytes. *Prog. Polym. Sci.* **2010**, *35*, 511–577.

7. Cope, A.C.; Mehta, A.S. Mechanism of the hofmann elimination reaction: An ylide intermediate in the pyrolysis of a highly branched quaternary hydroxide. *J. Am. Chem. Soc.* **1963**, *85*, 1949–1952.

8. Cope, A.C.; Trumbull, E.R. *Olefins from Amines: The Hofmann Elimination Reaction and Amine Oxide Pyrolysis in Organic Reactions*; R.E. Krieger Publication: Huntington, NY, USA, 1975.

9. Chempath, S.; Boncella, J.M.; Pratt, L.R.; Henson, N.; Pivovar, B.S. Density functional theory study of degradation of tetraalkylammonium hydroxides. *J. Phys. Chem. C* **2010**, *114*, 11977–11983.

10. Alikhani, M.; Moghbeli, M.R. Ion-exchange polyhipe type membrane for removing nitrate ions: Preparation, characterization, kinetics and adsorption studies. *Chem. Eng. J.* **2014**, *239*, 93–104.

11. Higa, M.; Tanaka, N.; Nagase, M.; Yutani, K.; Kameyama, T.; Takamura, K.; Kakihana, Y. Electrodialytic properties of aromatic and aliphatic type hydrocarbon-based anion-exchange membranes with various anion-exchange groups. *Polymer* **2014**, *55*, 3951–3960.

12. Dowding, P.J.; Goodwin, J.W.; Vincent, B. The characterization of porous styrene-glycidyl methacrylate copolymer beads prepared by suspension polymerization. *Colloids Surf. A Physicochem. Eng. Aspects* **1998**, *145*, 1–3.

13. Zhang, X.; Tanaka, H. Copolymerization of glycidyl methacrylate with styrene and applications of the copolymer as paper-strength additive. *J. Appl. Polym. Sci.* **2001**, *80*, 334–339.

14. Merle, G.; Wessling, M.; Nijmeijer, K. Anion exchange membranes for alkaline fuel cells: A review. *J. Membr. Sci.* **2011**, *377*, 1–35.

15. Wu, L.; Zhou, G.; Liu, X.; Zhang, Z.; Li, C.; Xu, T. Environmentally friendly synthesis of alkaline anion exchange membrane for fuel cells via a solvent-free strategy. *J. Membr. Sci.* **2011**, *371*, 155–162.

16. Lin, X.; Gong, M.; Liu, Y.; Wu, L.; Li, Y.; Liang, X.; Li, Q.; Xu, T. A convenient, efficient and green route for preparing anion exchange membranes for potential application in alkaline fuel cells. *J. Membr. Sci.* **2013**, *425–426*, 190–199.

17. Luo, Y.; Guo, J.; Wang, C.; Chu, D. Quaternized poly(methyl methacrylate-co-butyl acrylate-co-vinylbenzyl chloride) membrane for alkaline fuel cells. *J. Power Sources* **2010**, *195*, 3765–3771.

18. Wu, Y.; Wu, C.; Xu, T.; Yu, F.; Fu, Y. Novel anion-exchange organic-inorganic hybrid membranes: Preparation and characterizations for potential use in fuel cells. *J. Membr. Sci.* **2008**, *321*, 299–308.

19. He, S.S.; Frank, C.W. Facilitating hydroxide transport in anion exchange membranes via hydrophilic grafts. *J. Mater. Chem. A* **2014**, *2*, 16489–16497.

20. Elattar, A.; Elmidaoui, A.; Pismenskaia, N.; Gavach, C.; Pourcelly, G. Comparison of transport properties of monovalent anions through anion-exchange membranes. *J. Membr. Sci.* **1998**, *143*, 249–261.

21. Wang, J.; He, R.; Che, Q. Anion exchange membranes based on semi-interpenetrating polymer network of quaternized chitosan and polystyrene. *J. Colloid Interface Sci.* **2011**, *361*, 219–225.

22. He, R.; Li, Q.; Xiao, G.; Bjerrum, N.J. Proton conductivity of phosphoric acid doped polybenzimidazole and its composites with inorganic proton conductors. *J. Membr. Sci.* **2003**, *226*, 169–184.

23. Buchmüller, Y.; Wokaun, A.; Gubler, L. Fuel cell membranes based on grafted and post-sulfonated glycidyl methacrylate (GMA). *Fuel Cells* **2013**, *13*, 1177–1185.

24. Wu, Y.; Wu, C.; Gong, M.; Xu, T. New anion exchanger organic-inorganic hybrid materials and membranes from a copolymer of glycidylmethacrylate and γ-methacryloxypropyl trimethoxy silane. *J. Appl. Polym. Sci.* **2006**, *102*, 3580–3589.

25. Socrates, G. *Infrared Characteristic Group Frequencies: Tables and Charts*; Wiley: Hoboken, NJ, USA, 1994.

26. Cao, Y.C.; Wang, X.; Mamlouk, M.; Scott, K. Preparation of alkaline anion exchange polymer membrane from methylated melamine grafted poly(vinylbenzyl chloride) and its fuel cell performance. *J. Mater. Chem.* **2011**, *21*, 12910–12916.

27. Hasaninejad, A.; Shekouhy, M.; Golzar, N.; Zare, A.; Doroodmand, M.M. Silica bonded *N*-propyl-4-aza-1-azoniabicyclo[2.2.2]octane chloride (sb-dabco): A highly efficient, reusable and new heterogeneous catalyst for the synthesis of 4h-benzo[b]pyran derivatives. *Appl. Catal. A* **2011**, *402*, 11–22.

28. Nasef, M.M. Radiation-grafted membranes for polymer electrolyte fuel cells: Current trends and future directions. *Chem. Rev.* **2014**, *114*, 12278–12329.

29. Paddison, S.J.; Paul, R. The nature of proton transport in fully hydrated nafion®. *Phys. Chem. Chem. Phys.* **2002**, *4*, 1158–1163.

30. Choi, P.; Jalani, N.H.; Datta, R. Thermodynamics and proton transport in nafion i. membrane swelling, sorption, and ion-exchange equilibrium. *J. Electrochem. Soc.* **2005**, *152*, E84–E89.

31. Maurya, S.; Shin, S.H.; Kim, M.K.; Yun, S.H.; Moon, S.H. Stability of composite anion exchange membranes with various functional groups and their performance for energy conversion. *J. Membr. Sci.* **2013**, *443*, 28–35.

32. Varcoe, J.R.; Slade, R.C.T. Prospects for alkaline anion-exchange membranes in low temperature fuel cells. *Fuel Cells* **2005**, *5*, 187–200.

33. Ghigo, G.; Cagnina, S.; Maranzana, A.; Tonachini, G. The mechanism of the stevens and sommelet-hauser rearrangements. A theoretical study. *J. Org. Chem.* **2010**, *75*, 3608–3617.

34. Ye, Y.; Elabd, Y.A. *Polymers for Energy Storage and Delivery: Polyelectrolytes for Batteries and Fuel Cells*; American Chemical Society: Washington, DC, USA, 2012; p. 1096.

35. Agel, E.; Bouet, J.; Fauvarque, J.F. Corrigendum to "Characterization and use of anionic membranes for alkaline fuel cells": [Journal of Power Sources 101 (2001) 267–274]. *J. Power Sources* **2002**, *105*, 87.

36. Bauer, B.; Strathmann, H.; Effenberger, F. Anion-exchange membranes with improved alkaline stability. *Desalination* **1990**, *79*, 125–144.